Journal of the Indian Chemical Society 99 (2022) 100559

Contents lists available at ScienceDirect

Journal of the Indian Chemical Society

journal homepage: www.journals.elsevier.com/journal-of-the-indian-chemical-society

Magnetic separation of green synthesized Fe_3O_4 nanoparticles on photocatalytic activity of methyl orange dye removal

M.S. Manojkumar [a,*], K. Jeyajothi [b], A. Jagadeesan [c], V Jeevanantham [d]

[a] Department of Biotechnology, Vivekanandha College of Engineering for Women, Elayampalayam, Namakkal, 637 210, Tamilnadu, India
[b] Department of Petrochemical Engineering, Mahendra Institute of Engineering and Technology, Namakkal, 637 503, Tamilnadu, India
[c] Department of Mechanical Engineering, Mahendra Institute of Engineering and Technology, Namakkal, 637 503, Tamilnadu, India
[d] Department of Chemistry, Vivekanandha College of Arts and Sciences for Women (Autonomous), Elayampalayam, Namakkal, 637 205 Tamilnadu, India

ARTICLE INFO

Keywords:
X-ray techniques
Nanocrystalline materials
FTIR
Electron microscopy
Photo catalysis
Textile dyes

ABSTRACT

The most frequent method of removing malignant growth-causing tones from current effluents before releasing them into water sources such as rivers, lakes, and groundwater has become standard. Traditional waste-water treatment frameworks have trouble getting rid of these contaminants. This is a unique flavonoid that uses Fe_3O_4 nanorods as photocatalytic agents to corrupt material tone in the watery stage utilizing observable light enlightenment. Green technique was used to amalgamate CAF@Fe_3O_4 nanorod like gems. Disappearance of the bright (UV) maintenance top at 565 nm confirmed the elimination of Methyl orange tone. After 110 min, the sensational shading disposal of Fe_3O_4 nanorod was observed to be 100%. This is due to photochemical redox process and the use of Fe_3O_4 nanorods with a high energy gap of flavonoids. The findings show that Fe_3O_4 rod-like gems manufactured using green technology are extremely valuable in the photocatalytic annihilation of hazardous contaminants.

1. Introduction

In this materialistic world, the most noxious modern poisons are amalgamated to an exceptional degree in the ingredients used in food, beauty care products, cowhide, paper, and plastic industries to enhance its quality and shelf life. The majority of them are potentially toxic, posing an unprecedented threat to the present status of the environment. The tones were also commonly utilized in color creation [1–4] and in an intravenous blend that induces true mutagenesis and malignant growth-related diseases [5]. The most common physicochemical approaches include coagulation/flocculation, adsorption on initiated carbon, and layer filtration. In boondocks appealing, iron oxide nanoparticles (Fe_3O_4 NRs) have been used in a variety of applications, including recognition and separation of proteins to improve the affectability of attractive reverberation imaging (MRI), immunoassay, and designated drug conveyance [6,7]. In addition, nanoparticles have been employed in an amazing way in the fields of catalysis [8], proton trade layer, and biosensor [9]. Several iron oxides and their composites have demonstrated to be an excellent asset for shading debasement by adsorption [10,11] because of their large surface region to volume proportion and various nanostructures. Aqueous, sonochemical, miniature emulsion, electrochemical, sol-gel, and co-precipitation processes have all been used for the blend of Fe_3O_4 NRs [12,13]. The present study has involved the incorporation and employment of cassica auriculata bloom @ Fe_3O_4 NPs and uncovered their photocatalytic assessment and synergist activity upon methyl orange (MO) color removal in a watery medium (see Scheme 1).

2. Experimental method

The predetermined chemicals were utilized in De-ionized water without any additional sterilization.

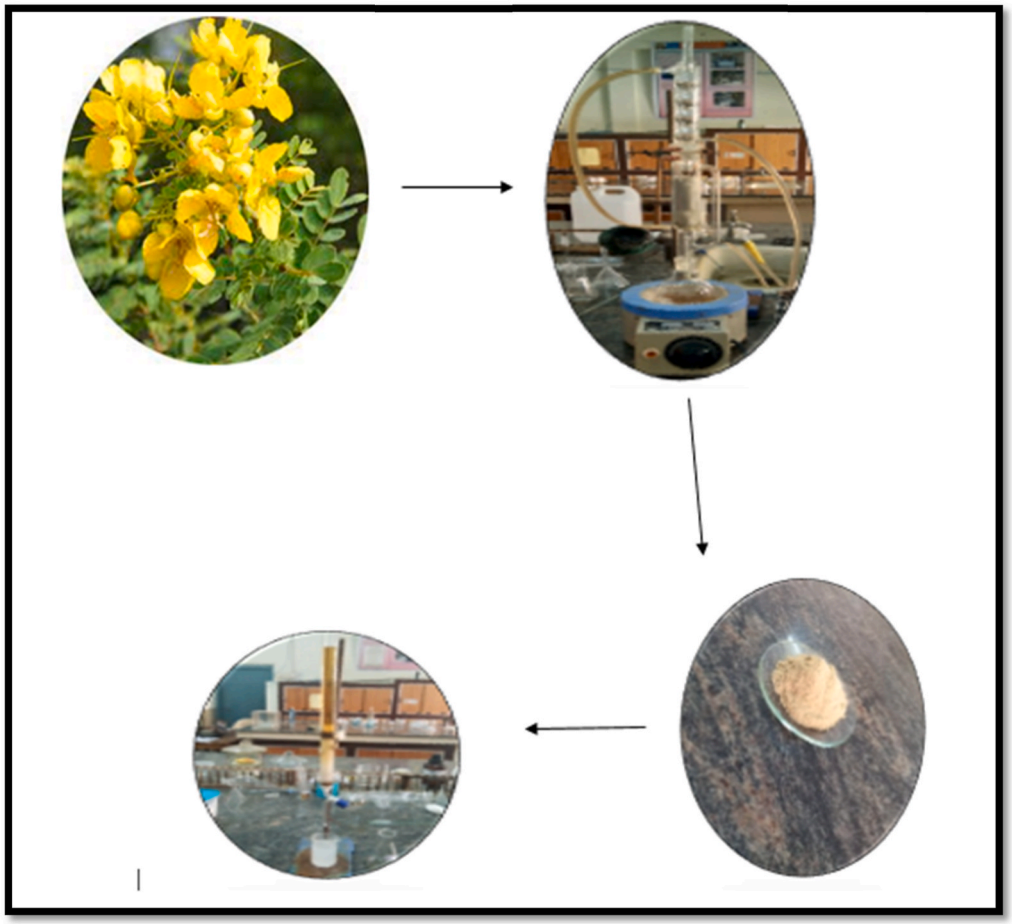
2.1. Preparation of bio-chelating agent

In the Soxhlet extruder, a soluble excavation of 5g CA powder was allowed to react with 60% methanol and 37% HCl. The acquired methanol extract was neutralized by 0.4mol Na_2CO_3 schemes, and the separated petroleum ether and ethyl acetate were dumped as multifold, where the outer surface was faded. Cassica auriculata flower extract

* Corresponding author.
E-mail addresses: manojkumar@vcew.ac.in (M.S. Manojkumar), hodpetro@miet.asia (K. Jeyajothi), hodmech@miet.asia (A. Jagadeesan), jeere06@gmail.com (V. Jeevanantham).

https://doi.org/10.1016/j.jics.2022.100559
Received 15 March 2022; Received in revised form 23 May 2022; Accepted 3 June 2022
Available online 8 June 2022
0019-4522/© 2022 Indian Chemical Society. Published by Elsevier B.V. All rights reserved.

(CAF) was fractionated using instinct series of dilutions. The total volume of the obtained solution was 30 ml, and column chromatography was used to fractionate them into six divisions. The obtained Flavonoids separates were evaluated by adding 0.5 ml hydroxide and blending the disassociated assessments, at room temperature. The yellow color observed confirmed the presence of flavonoids in the Cassica auriculata flower extract [11].



2.2. Architecture of recyclable Fe_3O_4 nanocatalyst

Fe_3O_4 MNRs were synthesized using a simple and eco-friendly method. The systematic approach is slightly modified [14]. The architecture of 2g $FeCl_3.6H_2O$ and 6.56 g sodium acetate were also used as bio-catalytic agent (flavonoid 50 ml) that were combined at 70 °C for 2 h, the homogeneous mixture became black and the obtained black product was then isolated [15,16].

2.3. Photo catalysis inspections (PCI)

The effect of flavonoid@Fe_3O_4NRs on textile color removal has been investigated using photo-catalysis framework. In the investigation, 50 ml of 0.1 M methyl orange (MO) dye was blended with 10 mg of Fe_3O_4NRs and exposed to UV light. A control (MO) set was also employed in the absence of a catalyst. The purpose of the feed solution was to maintain desorption equivalence to illuminate at regular intervals. Subsequently, the chromophoric group was decomposed in the presence of a catalyst under UV luminance (mercury lamp 120w) after exposing it over a range of time [13]. The decomposition of color was noticed due to the dramatic reduction of the absorption maximum at (max = 565 nm), as seen in Fig. 5. (a).

3. Results and discussion

3.1. Electronic spectra

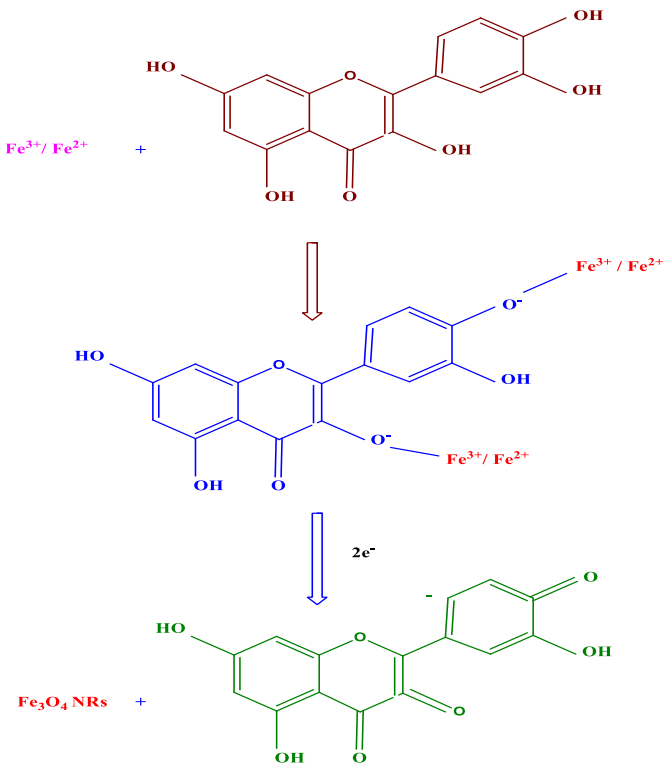
The electronic absorption bands of embedded Fe_3O_4NRs clearly showed two shoulder bands, with band I (Flavonoid) at 248 nm. The spectra for phenolic compounds and flavonoids are traditionally seen in the 210–290 nm range, and band II (Fe–O) observed at 402 nm was immobilized flavanols @ Fe_3O_4NRs, as seen in Fig. 1 (a). The mechanisms of formation of flavonoids (polyphenol group) containing Fe_3O_4NRs were displayed in Scheme 1. This was due to the emergence of Fe_3O_4NRs that was dependent on the crystallization growth mechanism [17]. In this regard, the functional group assembling flavonoid group was clearly characterized as it posses strong coordination, which was demonstrated by the Fourier transform infrared [FT IR] spectrum. The bandgap of Fe_3O_4NRs was elucidated by Tauc's interactions in Fig. 1 (b).

$$\alpha h\nu = C(h\nu - E_g)^2 \quad (1)$$

Flavonoid@Fe_3O_4 NRs had a band gap of 2.5 eV, suggesting a strong plasmonic effect and greater electrode potential of +33eV.

3.2. FT IR analysis

The appearance of broad peak at 3154 cm^{-1}, 2966-2228.7 cm^{-1}, 1545 cm^{-1}, 1399 cm^{-1}, 1016 cm^{-1} at 3154 cm^{-1} recommended as well as proved the appearance of the flavonoids as seen in Fig. 2(a) [18].

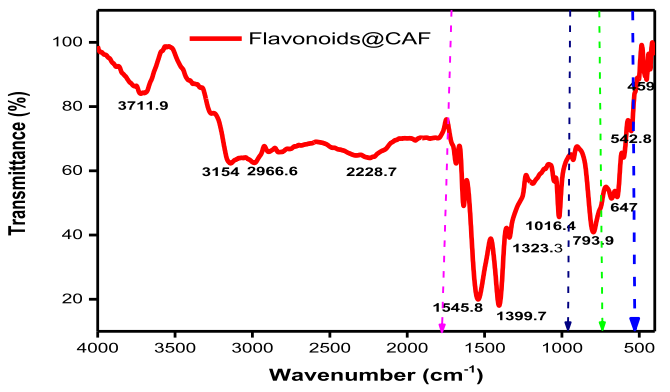


Scheme 1. Mechanisms of formation of Fe_3O_4 NRs using Flavonoids extracted from CAF extract.

Fig. 2 (b) illustrated that the FTIR characteristic peak for Fe_3O_4 nanorods was identified in 3469, 2094 and 1634 cm^{-1}. Surprisingly, other bands at 666 cm^{-1} were attributed to the typical extending vibrations of Fe–O bond [19]. Following that, the FTIR profile demonstrated the significant role of the flavonoids (polyphenolic) group in bioactive molecules, which reduced Fe^{3+}/Fe^{2+} metal ions and adapted Flavonoid @ Fe_3O_4NRs.

3.3. Crystal phase identification

The powder X-ray diffraction (XRD) study was used to determine the crystallite structure of Fe_3O_4 NRs. The XRD description of Fe_3O_4 NRs obtained using the flavonoid extract was shown in Fig. 3 (a) (CAF). The XRD results of Fe3O4 NRs revealed six significant strong reflection peaks at (200), (220), (311), (400), (422), (511), and (440), which were very



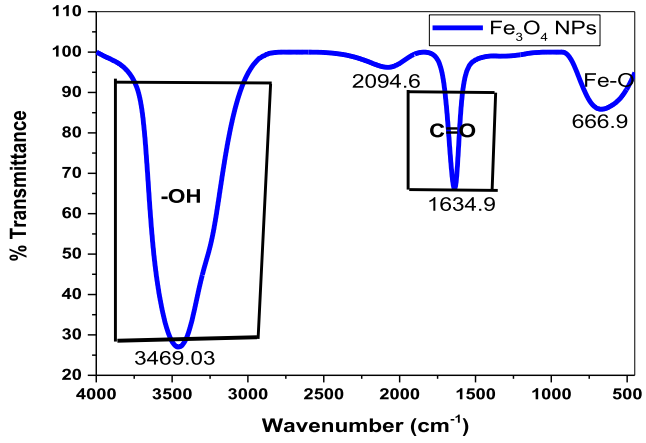


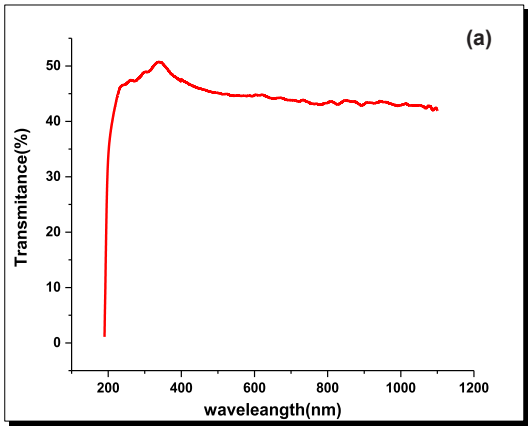
Fig. 2. (a) functional group spectrum of Flavonoid extracted from CAF extract **(b)** Functional group analysis of Fe_3O_4 nanorods using cassica auriculata flower extract.

well ordered to the cubic inverse spinal scheme of Fe3O4 NRs (JCPDS # 76-045), confirming the construction of Fe3O4NRs. Scherrer estimation [20,21] was used to calculate the size of the crystalline phase.

$$D = K\lambda / \beta \cos\theta \quad (2)$$

The calculated Fe_3O_4 NRs average crystallite size was 57.7 nm. Micro strain of Fe_3O_4 NRs was calculated by using the equation

$$\varepsilon = \beta \cos\theta/4 \quad (3)$$



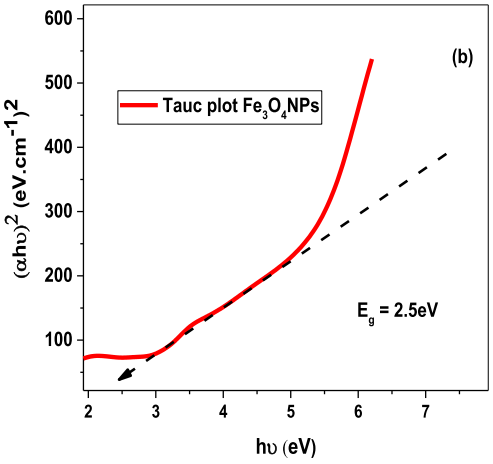


Fig. 1. (a) UV –DRS spectrum **(b)** Tauc plot of synthesized Fe_3O_4 NRs.

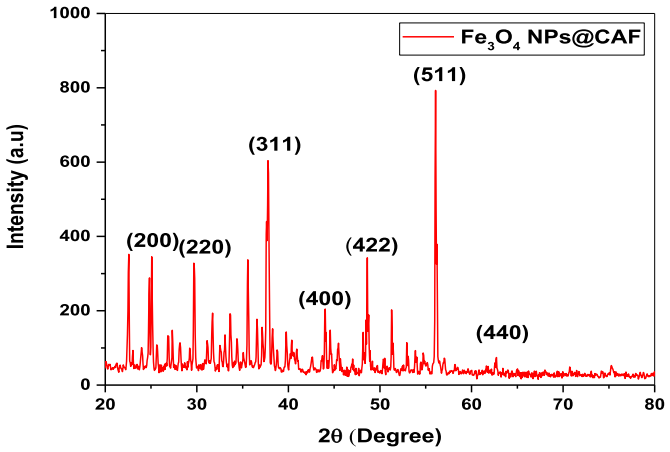


Fig. 3a. crystalline phase of synthesized Fe_3O_4 nanorods.

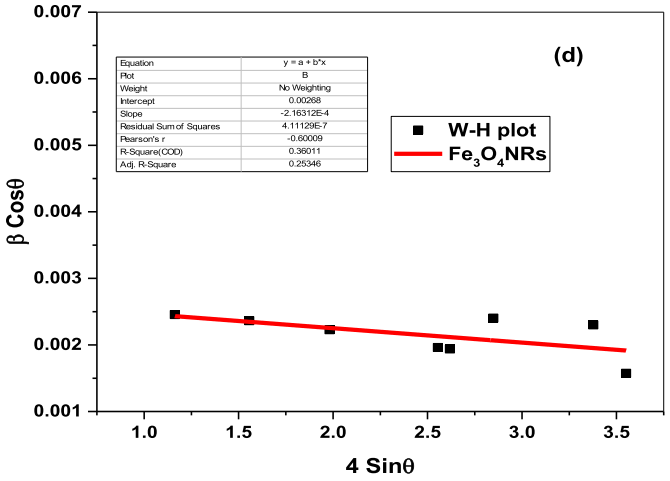


Fig. 3b. W–H plot of synthesized Fe_3O_4 nanorods using cassica auriculata flower extract.

Dis-location density was derived using the below mentioned equation

$$\delta = 1/D^2 \quad (4)$$

The micro strain of Fe_3O_4 NRs was 0.807 10-3, and the dislocation density was 8.751015. We could conclude from the outcomes that the potent bioactive dislocation density of crystallite size and quantum confinement divert has also aided in the colour cleanup process [22]. The W-H plot of Fe3O4 NRs were shown in Fig. 3 (b).

3.4. Morphological behavior of Fe_3O_4 nanoparticles

According to the electron microscopy (SEM) and transmission electron microscopy (TEM) assessment the size and surface morphology of the Fe_3O_4 NRs were affirmed to be wired, pole molded. Fig. 4(a) and (b) showed different amplifications of the SEM pictures of the Fe_3O_4 NRs which obviously demonstrated wire-like shapes. Fig. 4(c) showed TEM pictures of integrated Fe_3O_4 NRs which plainly portrayed bar like design. The mean size of the nanorods was noticed to be 15–20 nm. The bar like construction of Fe_3O_4 nanoparticles has instigated the solid ROS extremists that assist in photocatalytic movement [23,24].

3.5. BET isotherm spectra analysis

The interfacial area test Brunauer-Emmett-Teller (BET) was utilized to survey the interfacial district of Fe_3O_4 nanoparticles. Different outcomes like pore size and pore volume were inferred utilizing Barrett-Joyner-Halenda examination. The findings revealed that the created Fe_3O_4 NPs appeared to have a huge surface locale of 117.4 m^2 and 374.6 m^2g^{-1} with 10.50 nm pore size and 0.278 cm^3/g pore volume. Additionally, this would be viable for photocatalytic activity of methyl orange color (MO) debasement. [Fig. 5a] illustrates the adsorption-desorption isotherm plan chart of the combined Fe_3O_4 Nanoparticles [25].

3.6. EDS analysis

The EDS evaluation of the Fe_3O_4 was shown in Fig. 6(b), which clearly indicated the presence of Fe and O in the resulting material.

3.7. Magnetic properties of Fe_3O_4 by VSM analysis

Magnetic property of flavonoid @Fe_3O_4 NPs was estimated using a vibrating test magnetometer (VSM) at room temperature. The room temperature charge bend of the flavonoid @Fe_3O_4NPs was introduced as shown in Fig. 6(a). Neither coercivity nor hysteresis circles with remanence was noticed, which asserted the paramagnetic nature of flavonoid @Fe_3O_4NPs. The immersion polarization (Ms) values was noted as 65 emu/g at room temperature, which was lower than mass Fe_3O_4(92 emu/g) [26–28]. The lower Ms Value of flavonoid covered Fe3O4 NPs was attributed to the measure, surface effect and covering of non-attractive flavonoid on the outer layer of Fe_3O_4NRs.

3.8. Effect of pH

The influence of different pH (3, 5, 7, and 9) on the degradation efficiency of Methyl orange (MO) was investigated, which is shown in Fig. 8 (a). The effect of pH on the degradation of MO was examined by changing the pH from 3, 5, 7 and 9 at a fixed amount of catalyst (0.5 g/L) and constant MG concentration (10 mg/L). The change of color from deep yellow changes to colorless with a rapid decreased slight hypochromic shift which was found at 463 nm. It indicated that there would be a cleavage of the conjugated chromophore structure of the MO which would have occurred because of the formation of N-de-methylated intermediates.

In the acidic pH of 5, the absorption peak at 619 nm confirmed the adsorption of MO on Fe3O4 catalyst surface. It was found that degradation occurs (99.9%) within 110 min at pH 5. Thus, the efficiency of the degradation process was enhanced in the acidic medium, especially at pH 5. Thus, the acidic medium favors the complete degradation of MO on the catalyst surface.

3.9. Effect of catalyst dose

The amount of photocatalyst is another factor affecting the performance of the photocatalyst. The photocatalytic study was conducted under the conditions including source of irradiation, visible light, type of photocatalyst (Fe_3O_4photocatalyst), the weight of photocatalyst 0.1, 0.3, 0.5, 0.7 g/L and concentration of MO dye solution (1×10^{-5} M). The effect of the loading of Fe_3O_4 heterogeneous photocatalyst on degradation of MG dye is shown in Fig. 8(b). The results revealed that photocatalytic activity increased 80–99% after 110 min upon increasing the weight of the Fe_3O_4 photocatalyst from 0.1, 0.3, 0.5, 0.7 g/L. The degree of decomposition reaction increases with increase in the reactive sites on the catalyst, beyond which, it showed that the degradation process was reduced because of the scattering of light. There was a decrease in the penetration of light in the solution. When the amount of catalyst was higher in the solution, the activated molecules becomes deactivated by the collision of the lower energy molecules thereby increasing the turbidity of the medium and reducing the penetration of light leading to decrease in the reaction rate. Also, when the

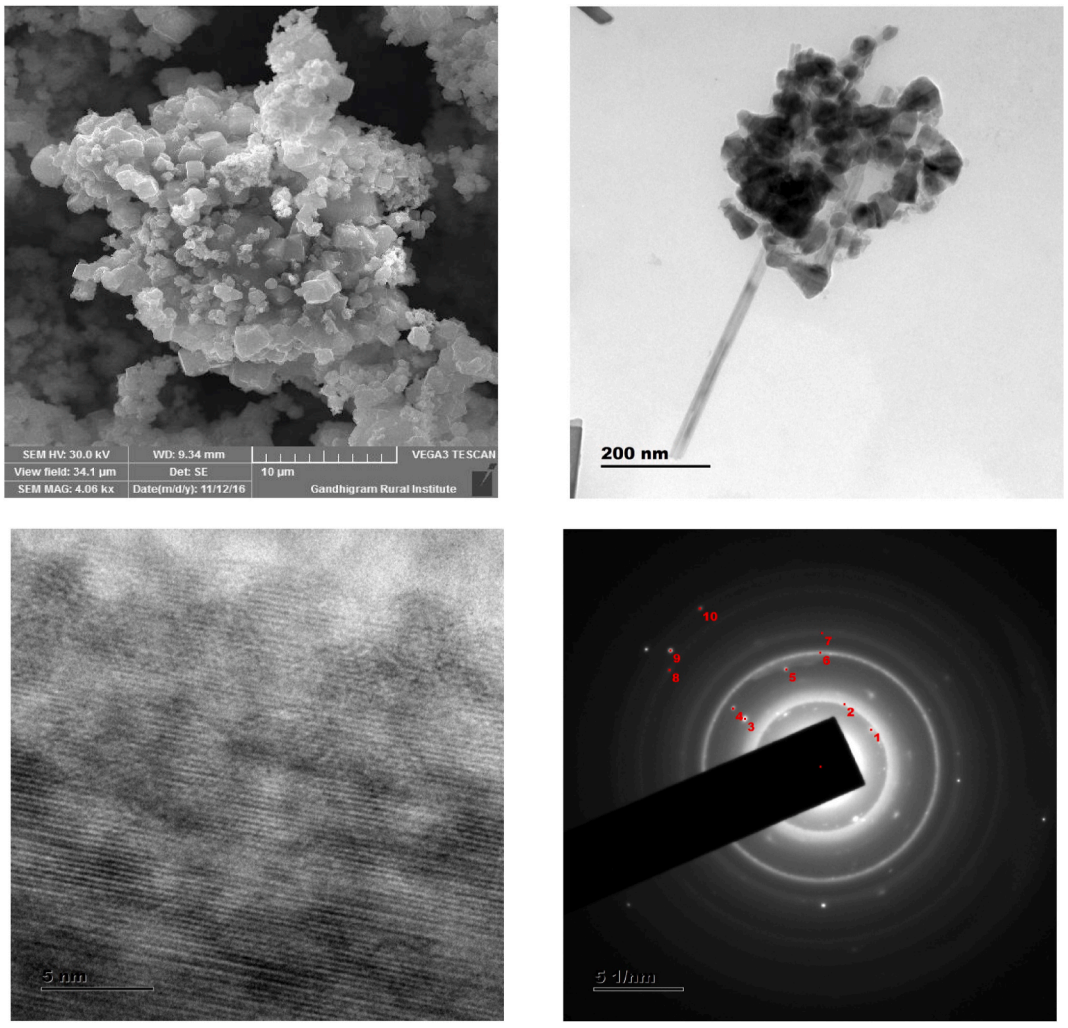


Fig. 4. (a) (b) Magnifications of the SEM images of the Fe_3O_4 NRs **(c)** TEM image of synthesized Fe_3O_4 NRs.

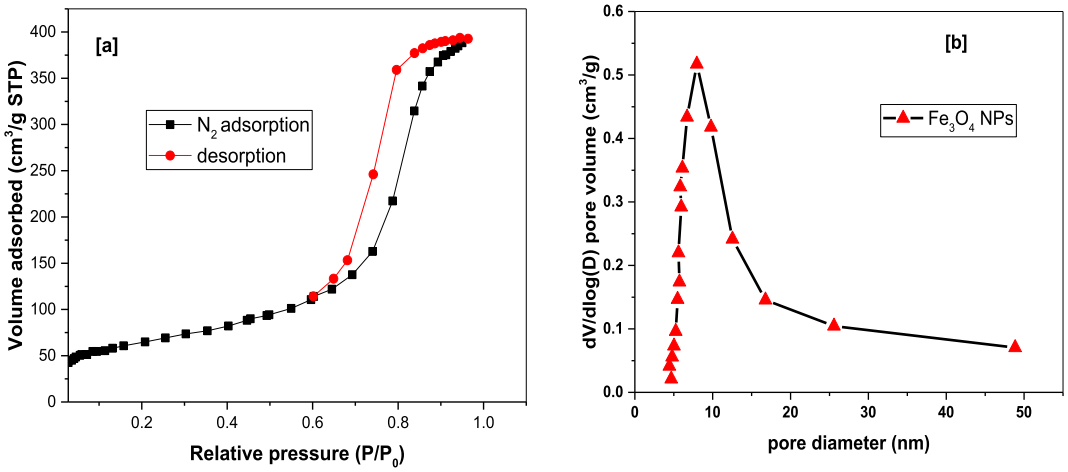


Fig. 5. (a) N_2 Adsorption-desorption isotherm analysis **(b)** pore volume vs pore diameter synthesized Fe_3O_4 nanoparticles.

photocatalyst absorbs the highest light the surface area becomes high, as a result of agglomeration at higher concentration of catalyst [29,30].

4. Kinetic model

The active conduct of Fe_3O_4 nanorods on methyl orange color was reviewed by photocatalytic technique (PCI) and Langmuir hinshelwood system as followed:

$$\ln (C/C_0) = \text{Kappt} \quad (5)$$

The plot of the diagram ln (C/C_0) versus time for the Fe_3O_4 NRs were viewed as 1.128 min^{-1} and furthermore pseudo first request dynamic

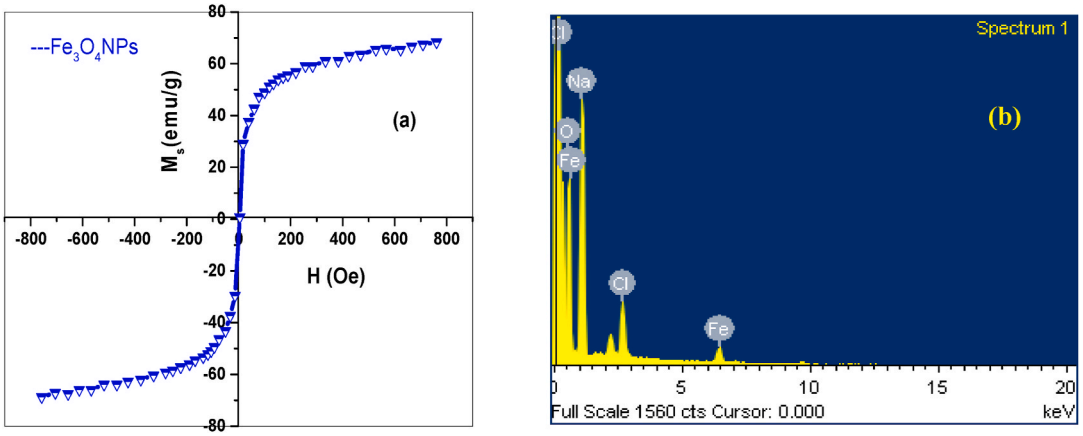


Fig. 6. (a) M − H properties of synthesized Fe_3O_4 nanorods **(b)** elemental spectrum of synthesized Fe_3O_4 nanorods.

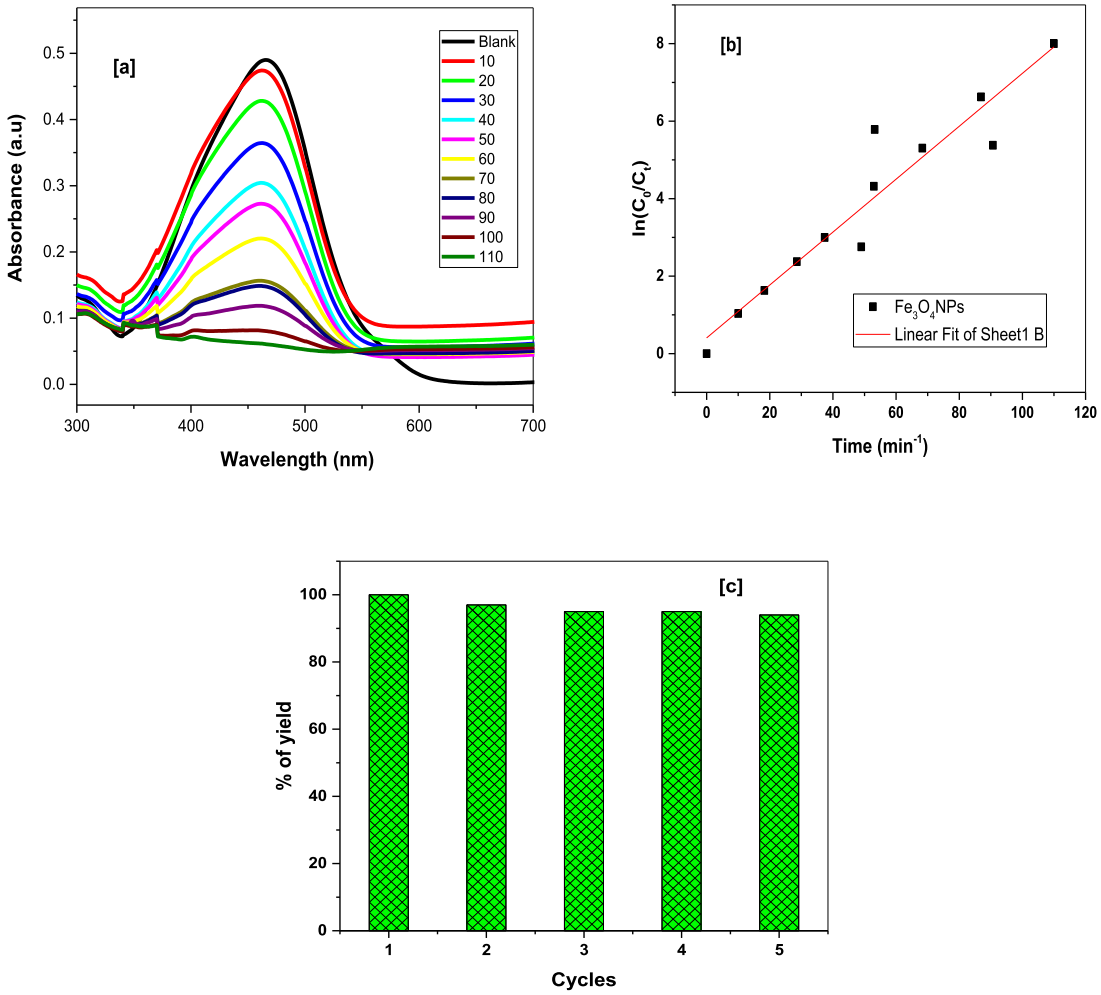


Fig. 7. (a) UV absorption spectrum of photocatalytic activity of methyl orange dye removal **(b)** kinetic plot of Fe_3O_4 nanorods **(c)** reusability graph of synthesized Fe_3O_4 nanorods. (For interpretation of the references to color in this figure legend, the reader is referred to the Web version of this article.)

model was displayed in Fig. 5 (b) [31,32].

4.1. Photocatalytic mechanism

When the material was exposed to light, there was excitation of electrons from VB to CB, and shaping the electron-openings in the VB. Moreover, the partition of charge and development of created charge was transported to surface of Fe_3O_4 layer and then directed to the redox interaction. The receptive oxygen (ROS) types of ($h + _{VB}$) in Flavonoid@Fe_3O_4nanorods are oxidation of methyl orange (MO) to responsive intermediates revolutionaries (*OH) that can change over into deterioration of water [13,21]. Degradation products such as CO_2, H_2O. Fig. 7(c) showed that the reusability and solidness of flavonoid@Fe_3O_4NRs were exceptionally steady which were assessed after

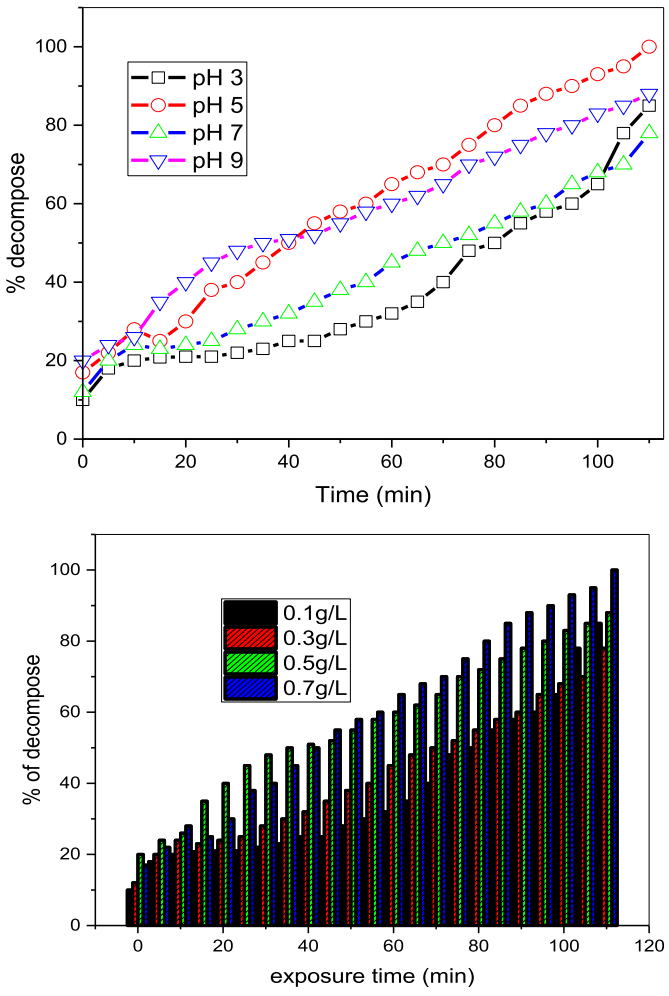


Fig. 8. (a) Effect of pH (b) Effect of catalytic dose.

five cycles with solid viable nature [33,34] and good photostability.

5. Conclusion

As a result, the flavonoids @Fe3O4NRs was effectively accomplished by greener way utilizing CR leaf extract. In this way, the recyclable and photograph steadiness of Fe_3O_4NRs were determined with different insightful portrayals. The magnetic properties of flavonoids covered Fe_3O_4nanorods were accomplished by the paramagnetic nature and the immersion charge (Ms) values that were viewed as 65 emu/g at room temperature. Moreover, the compelling color expulsion of flavonoid @Fe_3O_4NRs was seen to be 100% at 110 min which was due to solid dislocation-area thickness of 8.75×10^{15}, precious stone field fascination and responsive oxygen species (ROS) instrument that served additionally for quick response rate and simpler way to accomplish decolorization cycle fast. The photo catalyst was reused up to five cycles, which indicates the stability of the photo-catalyst.The flavonoid @Fe_3O_4NRs could be utilized as promising agent for polluted water and medicines, MRI, biosensors, and so on.

Funding

The authors declare that no funds, grants, or other support were received during the preparation of this manuscript.

Declaration of competing interest

The authors declare that there are no conflicts of interest.

Data availability

Data sharing not applicable to this article as no datasets were generated or analyzed during the current study.

References

[1] M.J.K. Ahmed, M. Ahmaruzzaman, M.H. Bordoloi, RSC Adv. 5 (2015) 74645–74655.
[2] ChangLiu JunyangYou, BowenLu XiFeng, XupinZhuang LeiXia, Carbohydr. Polym. 288 (2022), 119332, 15 July.
[3] Guobiao Li, Shouqiang Huang, Nanwen Zhu, Haiping Yuan, Dongdong Ge, J. Hazard Mater., Pub Date : 2020-09-15.
[4] Zahra Ansarian, Alireza Khataee, Samira Arefi Oskoui, Yasin Orooji, Hongjun Lin, Mater. Today Chem. 24 (June 2022), 100818.
[5] Hongming He, Qian-Qian Zhu, Ying Yan, Han-Wen Zhang, Zhan YeHan, Hongming Sun, Jing Chen, Cheng-Peng Li, Zhihong Zhang, Miao Du, Appl. Catal. B Environ. 302 (March 2022), 120840.
[6] Jing-Zhao Cheng, Zhi-Rong Tan, Yu-Qin Xing, Zhao-Qi Shen, Yu-Jie Zhang, Li-Lin Liu, Kai Yang, Long Chen, Shi-Yong Liu, Mater. Chem. 9 (2021) 5787–5795.
[7] M. Atarod, M. Nasrollahzadeh, S.M. Sajadi, RSC Adv. 5 (2015) 91532–91543.
[8] F. Barahuie, D. Dorniani, B. Saifullah, S. Gothai, M.Z. Hussein, A.K. Pandurangan, P. Arulselvan, M.E. Norhaizan, Int. J. Nanomed. 12 (2017) 2361–2372.
[9] B.R. Hao, R. Xing, Z. Xu, Y. Hou, S. Gao, S. Sun, Adv. Mater. 22 (2010) 2729–2742.
[10] D. Astruc, F. Lu, J.R. Aranzaes, Angew. Chem. 117 (2005) 8062–8083.
[11] I. Chourpa, L. Douziech-Eyrolles, L. Ngaboni-Okassa, J.F. Fouquenet, S. Cohen-Jonathan, M. Souce, H. Marchais, P. Dubois, Analyst 130 (2005) 1395–1403.
[12] R. Mirzajani, S. Ahmadi, J. Ind. Eng. Chem. 23 (2015) 171–178.
[13] X.M. Liang, L.J. Zhao, RSC Adv. 2 (2012) 5485–5487.
[14] O.A. Attallah, E. Girgis, M.M. Abdel-Mottaleb, J. Magn Mater. 399 (2016) 58–63.
[15] J.H. Wu, S.P. Ko, H.L. Liu, M.H. Jung, J.H. Lee, J.S. Ju, Y.K. Kim, Colloids Surf Physico Colloids Surf Physico. Chem. Eng. AspectsEng Aspects 313–314 (2008) 264–267.
[16] I.O. Macdonald, A.S. Oludare, Life Sci. 7 (2010) 3.
[17] Sada Venkates warlu, Bhajanthri Natesh Kumar, Bobbala Prathima, Yakkate Subba Rao, Nimmagadda VenkataVijayaJyothi, Arab. J. Chem. 9 (2014) 6.
[18] Santhanam Mohan, Manickam Vishnudevan, Green processing synth 8 (2019) 895–900.
[19] Sumit Arora, Itankar Prakash, Journal of Traditional and Complementary Medicine 8 (2018) 476e482.
[20] Van Thuan Le, Van Dat Doan, Thi Thanh Nhi Le, My Uyen Do, Thu-Thao Thi Vo, Ha Huu Do, Dinh Quoc Viet, Vy Anh Tran, Materials letter 283 (2021), 128749.
[21] S. Kaviya, J. Santhanalakshmi, B. Viswanathan, J. Muthumary, K. Srinivasan, SpectrochemicaActa Part A 79 (2011) 594–598.
[22] S. IrudayaMonisha, J. Rosaline Vimala, Biosci. Biotechnol. Res. Asia 15 (3) (2018) 687–698. September.
[23] Cheera Prasad, S. Karlapudi, P. Venkateswarlu, I. Bahadur, S. Kumar, J. Mol. Liq. 240 (2017) 322–328.
[24] Sada Venkateswarlu, Y. Subba Rao, T. Balaji, B. Prathima, N.V.V. Jyothi, Mater. Lett. 100 (2013) 241–244.
[25] A.S. Hassanien, B. Alaa, A. Aklcd, A.H. Sáaedi, CrystEngComm 20 (2018) 1716–1730.
[26] Azar Sadullahkhani, Irajkazeminezhad, Jun Lu ormerNur, Lars hulman, Magnuswillander, RSC Adv. 4 (2014) 36940–36950.
[27] Abdelmajid Lassoued, Mohamed Saber Lassoued, Brahim Dkhil, Salah Ammar, Abdellatif Gadri, J. Mater. Sci. Mater. Electron. (2018), 10854-018-8819-4.
[28] Naresh Kumar Sethy, Zeenat Arif, Pradeep Kumar Mishra, Pradeep Kumar, Green Process. Synth. 9 (2020) 171–181.
[29] Adeel Ahmed, Muhammad Usman, Bing Yua, Xin Ding, Qiaohong Penga, Youqing Shena, Hailin Conga, Adeel Ahmeda, Muhammad Usman, Bing Yua b, Dinga Xin, Qiaohong Penga, Youqing Shena, Hailin Conga, J. Photochem. Photobiol. B Biol. 202 (2020), 111682.
[30] Afshan Omidvar, Babak Jaleh, Mahmoud Nasrollahzadeh, Hamid Reza Dasmeh, Chemical Engineering Research and DesignVolume, 121, May 2017, pp. 339–347.
[31] Mahmoud Nasrollahzadeh, Mohaddeseh Sajjadi, S. Hamid Reza Dasmeh, Mohammad Sajadi, J. Alloys Compd. 763 (2018) 1024–1034, 30 September.
[32] Mahmoud Nasrollahzadeh, Samaneh Mahmoudi-GomYek, Motahharifar Narjes, Mostafa GhaforiGorab, Chem. Rec. 19 (12) (2019 Dec) 2436–2479.
[33] S. Kite, D.J. Sathe, K. Garadkar, Res. Chem. Intermed. 46 (2020) 1255–1282.
[34] Mangesh Kokate, Sudhir Dapurkar, Kalyanrao Garadkar, J. Anand Gole, Phys. Chem. C 119 (25) (2015) 14214–14223.